International Journal of Heat and Mass Transfer 52 (2009) 366–375

Contents lists available at ScienceDirect

International Journal of Heat and Mass Transfer

journal homepage: www.elsevier.com/locate/ijhmt

Transition from natural to mixed convection for steam–gas flow condensing along a vertical plate

Y. Liao [a], K. Vierow [b,*], A. Dehbi [a], S. Guentay [a]

[a] Laboratory for Thermal-Hydraulics, Paul Scherrer Institut, 5232 Villigen, Switzerland
[b] Department of Nuclear Engineering, Texas A&M University, MS 3133, College Station, TX 77843, USA

ARTICLE INFO

Article history:
Received 29 July 2007
Received in revised form 22 March 2008
Available online 25 July 2008

Keywords:
Mixed convection
Condensation
Non-condensable gases

ABSTRACT

An analysis method based on two-phase boundary layer analysis has been developed to study the effects of superimposed forced convection on natural convection steam–gas flow condensing along a vertical plate. The mechanism by which superimposed forced convection enhances heat transfer is evaluated: the bulk flow blows away non-condensable gases accumulating near the interface, resulting in an elevated condensation driving force. Further, this bulk flow blowing capability may be characterized by a conventional mass transfer driving potential. Results of the new model are shown to be consistent with experimental data. Finally, a simple criterion was developed to identify transition to mixed convection from natural convection steam–gas flow.

1. Introduction

Condensation from steam–gas mixtures along a vertical plate has important applications in nuclear engineering design and safety analysis. In the new generation of light water reactors, the reactor containment integrity under postulated accident conditions is ensured by condensation of steam–gas mixtures along vertical surfaces inside the containment building and vaporization of water outside the containment (Fig. 1). This heat removal process relies only on naturally occurring processes and hence achieves a high safety level for the containment. Due to its importance, an abundance of theoretical and experimental work has been carried out to investigate condensation from steam–gas flow along a vertical plate. The analytical work is summarized below.

Theoretical analysis using boundary layer approximations began with Sparrow's pioneering work [1], in which the gas-phase flow was regarded as natural convection and the two-phase boundary layer equations were solved with the similarity method. Minkowycz investigated a number of important effects in natural convection condensation of steam–gas flow [2]. However, it will be shown in this paper that treating an actual flow in the experimental work as natural convection can produce a large error. In the current work, the gas-phase flow is considered as a mixed convection flow, in which the basic natural convection component is caused by the gravitational force and the density difference resulting from variations of gas composition and temperature across the boundary layer, while the superimposed forced convection component is caused by the induced bulk velocity (Fig. 1). Although a given mixed convection flow may be dominated by the natural or forced convection component, the current work focuses on the former case and investigates the condition under which transition to mixed convection can be considered to take place from natural convection steam–gas flow condensing along a vertical plate.

An important problem associated with mixed convection is the identification of convection regimes and conditions under which a mixed convection process is distinct from a natural or forced convection process, since solving this problem aids in the selection of a convection-regime dependent heat transfer correlation in engineering calculations employing the heat and mass transfer analogy approach. For single-phase heat transfer, this problem has already been solved [3,4].

For condensation of steam in the presence of a non-condensable gas, the conventional method for convection regime identification solves two-phase multi-component conservation equations with finite difference approximations and determines how the variations of the many input variables can lead to a change of convection regime. Denny [5,6] studied the effects of the bulk velocity using finite difference approximations and found that the bulk velocity enhances condensation heat transfer of the basic natural convection process. However, the mechanism of heat transfer enhancement by the bulk velocity was not investigated and the convection regime was not discussed. In Debbissi's [7] work, the effects of the bulk velocity on water evaporation into humid air from a vertical wetted plate was investigated. Debbissi found that increasing the bulk velocity reduces the thickness of the mass boundary layer. While the current work considers the condensation process, the governing equations are the same as those in

* Corresponding author. Tel.: +1 979 458 0600; fax: +1 979 845 6443.
E-mail address: vierow@ne.tamu.edu (K. Vierow).

0017-9310/$ - see front matter © 2008 Elsevier Ltd. All rights reserved.
doi:10.1016/j.ijheatmasstransfer.2008.06.008

Nomenclature

B_m	mass transfer driving potential in Eq. (30);
c_p	specific heat
D	diffusivity
f	dimensionless stream function in Eq. (7);
g	gravity constant
Gr^*	gx^3/v^2
Gr	$\beta^+(W_i - W_\infty)Gr^*$, Grashof number
h	condensation heat transfer coefficient in Eq. (15)
h_{fg}	latent heat
L	plate length
M	molecular weight
$\dot{m}$	local condensation mass flux in Eq. (13)
P	pressure
Pr	Prandtl number
q	condensation heat flux
Re	$u_\infty x/v$, Reynolds number
Sc	Schmidt number
T	temperature
$\overline{T}$	average temperature
u	longitudinal velocity
v	transverse velocity
v_{fg}	differential specific volume
W	gas mass fraction
x	longitudinal coordinate
x_v	steam volumetric fraction
y	transverse coordinate

Greek symbols

β	volumetric coefficient of thermal expansion
β^*	volumetric coefficient of expansion with concentration in Eq. (5)
β^+	volumetric coefficient in Eq. (28)
δ	liquid film thickness
η	similarity variable in Eq. (6)
μ	absolute viscosity
v	kinematic viscosity
ξ	mixed convection parameter in Eq. (6)
ρ	density
ϕ	differential gas mass fraction in Eq. (8)
Ψ	stream function in Eq. (7).

Subscripts

g	gas
i	two-phase interface
L	liquid-phase
m	mixture
t	total
v	steam
w	wall
δ	two-phase interface
∞	gas bulk

Debbissi's work, except that the role of steam and air are interchanged. The presence of a bulk velocity assisting natural convection condensation will be shown to similarly reduce the thickness of the mass boundary layer. Lucas [8] tried to obtain a method for convection regime identification, but realized that no solution could be found, possibly due to a large number of independent variables used in the finite difference method and thus too much complexity involved in the analysis. Srzic [9] employed the same mixed convection parameter as used by Lucas [8] to transform the conservation equations. The variation of detailed heat transfer results with a mixed convection parameter, temperature difference and gas concentration were presented, however, the only conclusion about transition to mixed convection that could be drawn was that the mixed convection effect depends on a number of variables. Recent studies [10,11] on condensation with a non-condensable gas employing boundary layer analysis concentrated on different flow configurations, the effects of turbulence, liquid-phase inertia and energy convection, and also on solving the full boundary layer equations. None of these recent studies discussed the problem of convection regime identification.

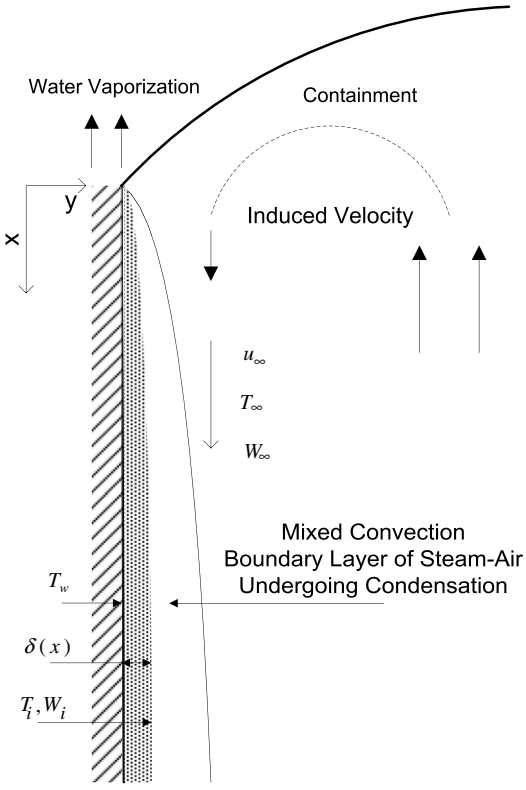

Fig. 1. Mixed convection of steam–air flow undergoing condensation inside containment.

In the current work, the mixed convection effects are represented by a dimensionless parameter which is a function of the relative magnitude of forced convection indicated by the Reynolds number to natural convection indicated by the Grashof number, Re^2/Gr. Upon introducing this dimensionless parameter, the multi-component two-phase conservation equations can reduce to simpler forms and the analysis becomes manageable.

The present investigation was undertaken to fulfill two complementary objectives. The first is to study heat transfer effects of superimposed forced convection on the basic natural convection process of steam–gas flow undergoing condensation along a vertical plate and to compare analytical heat transfer results with a variety of experimental data. The second is to investigate conditions under which transition to mixed convection takes place for such a natural convection steam–gas flow. The gas-phase conservation equations will be coupled herein to the liquid-phase equations through interfacial relations and solved using the local similarity method [12] to reduce the conservation equations into ordinary differential equations. The local similarity as well as local non-similarity [13] approximations are conventionally used for mixed

convection heat transfer analysis of single-phase flow [4] and later applied to analysis of condensation with a non-condensable gas [14], and mixed convection condensation of pure steam [15]. The local similarity method is preferred in the current study not only due to its simplicity in numerical solutions, but also due to dimension reduction of the multi-variable problem by introducing dimensionless groups in the transformation of conservation equations.

While the current work studies mixed convection from the perspective that mixed convection is viewed as a basic natural convection process superimposed with varying amount of forced convection, mixed convection can also be viewed as a basic forced convection process superimposed with varying amount of natural convection. Forced convection condensation in the presence of a non-condensable on a horizontal plate was first studied by Sparrow [16] and recently by Volchkov [17]. The classic work [16] neglected the liquid film inertia and energy convection to solve the two-phase boundary equations with the similarity method. The recent work [17] neglected the liquid film thermal resistance and then solved the gas-phase boundary equations using the finite difference method to investigate the validity of the Reynolds analogy under varying conditions with a variety of gas concentrations. In both studies, the effects of superimposed natural convection on forced convection condensation could not be investigated, since the axial pressure gradient induced by the density difference resulting from the non-uniform temperature and concentration distribution [18] was omitted in the longitudinal momentum equation.

2. Analysis

Fig. 1 shows the coordinate system used to set up the boundary layer equations. The longitudinal coordinate (x) is measured vertically downward along the plate, and the transverse coordinate (y) is normal to the plate and measured rightward. The free stream with a temperature (T_∞) and gas mass fraction (W_∞), is condensed along the two-phase interface with an unknown temperature (T_i) and gas mass fraction (W_i). The cooling surface of the wall has a constant temperature (T_w). The liquid film thickness, $\delta(x)$, varies with the longitudinal length. If the bulk gas is stagnant, it is treated in Sparrow's work [1] as pure natural convection condensation. However, in most cases a longitudinal bulk velocity (u_∞) is induced and the behavior of the otherwise natural convection boundary layer will change due to superimposed forced convection. One of the tasks in the current work is to investigate the conditions under which the induced bulk velocity would significantly influence the basic natural convection process.

As a common practice in convection regime identification for single-phase flow [3,4], turbulence is not considered in the current analysis either. In the current studies of transition from natural to mixed convection, both the natural and the forced convection components are of moderate magnitude: for the gas mixture flow along a flat plate, the maximum values of Re and $\sqrt{Gr}$ considered in the current work are on the order of 5×10^4. Furthermore, Shekriladze [19] pointed out that suction induced by the transverse condensation velocity stabilizes the laminar boundary layer and delays transition to turbulence. Therefore, two laminar boundary layers are considered: the condensate layer adjacent to the vertical flat plate surface and the steam–gas layer between the condensate layer and the bulk flow. The key unknown variable governing condensation heat transfer is the interfacial temperature, which is determined by the interaction between the liquid film and the steam–gas mixture. The current analysis is only valid for the induced bulk flow co-current to the basic buoyancy flow, namely, the induced bulk velocity assisting heat transfer for the basic buoyancy flow.

2.1. Gas-phase boundary layer

Species conservation for the gas component:

$$\frac{\partial u}{\partial x}+\frac{\partial \upsilon}{\partial y}=0 \tag{1}$$

Species conservation for the gas component:

$$u\frac{\partial W}{\partial x}+\upsilon\frac{\partial W}{\partial y}=D\frac{\partial^2 W}{\partial y^2} \tag{2}$$

Momentum conservation:

$$u\frac{\partial u}{\partial x}+\upsilon\frac{\partial u}{\partial y}=\frac{\rho-\rho_\infty}{\rho}g+\nu\frac{\partial^2 u}{\partial y^2} \tag{3}$$

where the original term, $-\rho^{-1}\partial p/\partial x+g$, on the right hand side is replaced by the buoyancy force term, $g(\rho-\rho_\infty)/\rho$. Using the Boussinesq approximation, density variations are considered only to the extent that they contribute to the buoyancy force, while variations in other fluid properties are not considered. The concentration contribution to the buoyancy force can be written from the ideal gas law as [1]

$$\frac{\rho-\rho_\infty}{\rho}=1-\frac{M_{m\infty}}{M_m}=\beta^*(W-W_\infty) \tag{4}$$

Upon applying the definition of the mixture molecular weight, the volumetric coefficient of expansion with concentration can be expressed as

$$\beta^*=\frac{M_g-M_v}{M_g-(M_g-M_v)W_\infty} \tag{5}$$

It is noted that in Sparrow's work [1] the contribution of thermal expansion to the buoyancy force was neglected, which is only valid when thermal expansion is negligible in comparison with volumetric expansion caused by composition variations. To compare with Sparrow's work the simplified buoyancy force in Eq. (4) is adopted until in a later section where the contribution of thermal expansion to the buoyancy force will be considered. The energy equation is not considered since sensible heat transfer is negligible compared to condensation heat transfer of saturated vapor.

As a starting point, a new coordinate system is defined in the current work as

$$\xi=\frac{1}{1+\left(\frac{Re^2}{Gr^*}\right)^{1/4}},\quad \eta=\frac{y-\delta(x)}{x^{1/4}\xi}\left(\frac{g\beta^*}{4\nu^2}\right)^{1/4} \tag{6}$$

where $Re=u_\infty x/\nu$ and $Gr^*=gx^3/\nu^2$. This coordinate system is introduced analogous to that used in analysis of mixed convection for single-phase heat transfer [20] and pure steam condensation [15]. Nevertheless, the new system is unique since it is used to treat physical processes different from the previous ones. The dimensionless group, ξ, ranging from 0.0 to 1.0, is the mixed convection parameter in the current analysis and represents the varying degree of bulk velocity (forced convection) effects on the basic natural convection process. If the bulk flow is stagnant ($\xi=1$), the process is pure natural convection. With gradual increase of the bulk velocity, the forced convection component represented by the Reynolds number becomes more significant relative to the natural convection component represented by the Grashof number and the value of ξ decreases toward zero. The dimensionless distance from the two-phase interface (η) is expressed in a way to be consistent with the stream function to obtain a local similarity transformation. The similarity variable (η) which is a combination of the x and y variables will be used later to express the velocity or concentration profile as a function of a single variable.

Next, a stream function

$$\Psi(x,y)=\frac{4\nu x^{3/4}}{\xi}\left(\frac{g\beta^*}{4\nu^2}\right)^{1/4}f(\xi,\eta) \tag{7}$$

and a gas mass fraction variable

$$\phi=W-W_\infty \tag{8}$$

are introduced herein with regard to the new coordinate system to transform the momentum and species conservation equations from the (x,y) system to the (ξ,η) system. To solve the transformed equations, the local similarity method [12,13,20] is preferred in the current study not only due to its simplicity in numerical solutions, but also due to reduced complexity of the multi-variable problem by introducing dimensionless groups in the transformation of conservation equations.

In the local similarity method [12,13,20], terms in the transformed equations involving derivatives with respect to the mixed convection parameter (in the current work, ξ) are truncated; at any longitudinal position, the local mixed convection parameter is regarded as an assignable parameter. Consequently, the thus-transformed boundary layer equations will be treated as a system of ordinary differential equations at each local position of interest. If the first order derivatives with respect to the mixed convection parameter are retained but higher order derivatives are truncated, the method is termed the local non-similarity method [13]. Certainly finite difference approximations can also be used, but this method involves a large number of independent variables and may be inappropriate in previous studies [8] trying to identify convection regimes. The approximations of the local similarity or non-similarity method were found to have sufficient accuracy compared to the finite difference numerical method [20]. In accordance with the local similarity method, transformation of the conservation equations was carried out [21], and the major results are reported below.

Longitudinal velocity:

$$u=\frac{2}{\xi^2}(gx\beta^*)^{1/2}f' \tag{9}$$

Transverse velocity:

$$\upsilon=-\left(\frac{g\beta^*}{4\nu^2}\right)^{1/4}\frac{\nu}{x^{1/4}\xi}\left[(2+\xi)f+4xf'\frac{\partial\eta}{\partial x}\right] \tag{10}$$

Momentum conservation equation:

$$f'''-2\xi f'^2+(2+\xi)ff''+\xi^4\phi=0 \tag{11}$$

Species conservation equation:

$$\frac{1}{Sc}\phi''+(2+\xi)f\phi'=0 \tag{12}$$

where the primes denote differentiation with respect to the similarity variable (η).

Sparrow's analysis [1] on natural convection condensation is noted to be a specific case of the current one. For natural convection flow, it follows that $Re^2/Gr^*=0$ ($\xi=1$) and hence the transformed equations, (11) and (12), reduce to those derived by Sparrow [1]. If $Re^2/Gr^*>0$ ($0<\xi<1$), the bulk velocity effects come into play herein as a superimposed forced convection process. Therefore, investigation of a varying degree of the bulk velocity effects on the basic natural convection process will be carried out in the current work by solving Eqs. (11) and (12) with a varying mixed convection parameter (ξ).

2.2. Liquid-phase boundary layer

Sparrow [1] simplified the liquid-phase conservation equations by neglecting inertia and energy convection and solved the system subject to the boundary conditions that $u=\upsilon=0$, $T=T_w$ at the wall ($y=0$), and $T=T_i$, $\partial u/\partial y=0$ at the interface ($y=\delta$). Some of the solutions are replicated below since they will be used later in the gas-phase closure equations.

Local condensation mass flux:

$$\dot{m}=\frac{q}{h_{fg}}=\frac{\mu_L}{x}\left[\frac{c_{pL}(T_i-T_w)}{h_{fg}Pr_L}\right]^{3/4}\left(\frac{gx^3}{4\nu_L^2}\right)^{1/4} \tag{13}$$

Interface longitudinal velocity:

$$u_\delta=\left[\frac{c_{pL}(T_i-T_w)}{h_{fg}Pr_L}\right]^{1/2}(gx)^{1/2} \tag{14}$$

The average condensation heat transfer coefficient for the whole plate and defined from the gas bulk to the wall can be derived from Eq. (13) as

$$h=0.943\frac{h_{fg}\mu_L}{T_\infty-T_w}\left[\frac{c_{pL}(T_i-T_w)}{h_{fg}Pr_L}\right]^{3/4}\left(\frac{g}{L\nu_L^2}\right)^{1/4} \tag{15}$$

Condensation heat transfer is fully determined when the interfacial temperature (T_i) is obtained from solution of the gas-phase equations.

2.3. Gas-phase closure equations

Five closure conditions are required to solve the gas-phase equations, Eqs. (11) and (12). The first two conditions are specified by the velocity and gas mass fraction in the bulk. At infinity ($y=\infty$), the longitudinal velocity is specified with the bulk velocity ($u=u_\infty$). Upon substituting $y=\infty$ and $u=u_\infty$ into Eq. (9), and using the ξ definition in Eq. (6) it is derived herein that

$$f'(\infty)=\frac{(1-\xi)^2}{2\beta^{*1/2}} \tag{16}$$

At infinity ($y=\infty$), the gas mass fraction is specified by the bulk gas mass fraction ($W=W_\infty$). Upon substituting $y=\infty$ and $W=W_\infty$ into Eq. (8), it follows that

$$\phi(\infty)=0 \tag{17}$$

The next two closure equations can be derived from the two-phase interfacial relations: conservation of mass and continuity of velocity.

The mass flux crossing the interface evaluated from the gas-phase is

$$\dot{m}=\rho\left(u_\delta\frac{d\delta}{dx}-\upsilon_\delta\right) \tag{18}$$

where the gas longitudinal velocity at the interface is evaluated using Eq. (9),

$$u_\delta=\frac{2}{\xi^2}(gx\beta^*)^{1/2}f'(0) \tag{19}$$

and the gas transverse velocity at the interface is evaluated from Eq. (10),

$$\upsilon_\delta=-\left(\frac{g\beta^*}{4\nu^2}\right)^{1/4}\frac{\nu}{x^{1/4}\xi}\left[(2+\xi)f(0)+4xf'(0)\left.\frac{\partial\eta}{\partial x}\right|_{y=\delta}\right] \tag{20}$$

Upon using $\partial\eta/\partial x|_{y=\delta}=-(x^{1/4}\xi)^{-1}\ [g\beta^*/(4\nu^2)]^{1/4}d\delta/dx$, which is derived from the definition of the similarity variable (η) in Eq. (6), and substituting Eqs. (19) and (20) into Eq. (18), the mass flux evaluated from the gas-phase is found to be

$$\dot{m}=\frac{\rho\nu(2+\xi)}{x^{1/4}\xi}\left(\frac{g\beta^*}{4\nu^2}\right)^{1/4}f(0) \tag{21}$$

From the interfacial relation for mass conservation, the third closure equation is derived herein using Eqs. (13) and (21) as

$$f(0)=\frac{\xi}{(2+\xi)\beta^{*1/4}}\left[\frac{c_{pL}(T_i-T_w)}{h_{fg}Pr_L}\right]^{3/4}\left(\frac{\rho_L\mu_L}{\rho\mu}\right)^{1/2} \tag{22}$$

Next, upon using the interfacial relation of continuity of velocity, the fourth closure equation is derived herein using Eqs. (14) and (19) as

$$f'(0)=\frac{\xi^2}{2\beta^{*1/2}}\left[\frac{c_{pL}(T_i-T_w)}{h_{fg}Pr_L}\right]^{1/2} \tag{23}$$

The fifth closure equation is obtained from the assumption of an interface impermeable to the gas component. Since the interfacial gas mass flux is zero, the convective mass flux component is balanced by the diffusive mass flux component

$$\rho_g\left(u_\delta\frac{d\delta}{dx}-v_\delta\right)=-\rho D\frac{\partial W}{\partial y}\bigg|_{y=\delta} \tag{24}$$

Upon using Eqs. (19), (20), and (24), the fifth closure equation becomes

$$\phi'(0)=-(\phi(0)+W_\infty)Sc(2+\xi)f(0) \tag{25}$$

It is noted that for pure natural convection flow ($\xi=1$), the five closure equations derived in the current work reduce to those derived by Sparrow [1]. If $0<\xi<1$, the mixed convection effects come into play in the closure conditions for the gas-phase equations.

2.4. Solution method

The ultimate goal of solving the gas-phase equations in Eqs. (11) and (12), subject to associated closure equations in Eqs. (16), (17), (22), (23), and (25) is to obtain the interfacial temperature (T_i), which can be assumed equal to the local steam saturation temperature corresponding to the steam partial pressure therein. The steam partial pressure at the interface can be inferred from the gas mass fraction at the interface (W_i), which is readily available when $\phi(0)$ is resolved ($W_i=\phi(0)+W_\infty$) as part of the solution. However, the right hand side of the two closure equations in Eqs. (22) and (23) contain the unknown interfacial temperature, therefore an iterative method was devised.

First, the mixed convection parameter (ξ) is assigned a value between 0.0 and 1.0, depending on the magnitude of superimposed forced convection of interest. Next, the initial value of the interfacial temperature is assigned as the mean of the wall and the gas bulk temperatures. Finally, the gas-phase equations subject to the closure equations are solved with the approximate interfacial temperature and the procedure is repeated until the interfacial temperature converges. The condensation heat transfer coefficient is readily available by substituting the converged interfacial temperature into Eq. (15).

2.5. Contribution of thermal expansion to buoyancy force

To achieve a similarity method, Sparrow [1] neglected the contribution of thermal expansion to the buoyancy force. Gebhart [22] estimated that under ambient conditions, the contribution from a temperature difference of 10.0 °C to the buoyancy force is about one-third of that from the concentration difference. The temperature contribution would be higher as the temperature difference becomes larger and thus also important to generating the buoyancy force. Therefore, an approximate method to account for the temperature contribution to the buoyancy force is derived herein without violating the similarity assumption.

Upon retaining the linear terms of differential temperature and concentration, and neglecting terms with higher orders, the buoyancy force can be approximated as [22]

$$\frac{\rho-\rho_\infty}{\rho}=\beta^*(W-W_\infty)+\beta(T_\infty-T) \tag{26}$$

Treating fluid temperature as an explicit independent variable is incompatible with the current similarity method, wherein the fluid temperature has been decoupled from the conservation equations by omitting sensible heat transfer. Nevertheless, the second term on the right hand side of Eq. (26) representing the temperature contribution to the buoyancy force is a function of the first term representing the concentration contribution. In Appendix A, by using the Clausius–Clapeyron equation, the explicit dependence of the buoyancy force on fluid temperature difference was rewritten in terms of gas mass fraction difference. The ratio of the temperature contribution to the concentration contribution can be derived herein upon comparing Eqs. (26) and (A4) as

$$\frac{\beta(T_\infty-T)}{\beta^*(W-W_\infty)}\approx\frac{M_{m\infty}}{M_g-M_v}\frac{P_t v_{fg}}{h_{fg}} \tag{27}$$

Fig. 2 shows that the term on the right hand side of Eq. (27) without the explicit dependence on fluid temperature is a reasonable approximation to the term on the left hand side. The curves in Fig. 2 were plotted for a typical steam–air mixture with a total pressure of 2.0 bar, a bulk air mass fraction of 0.5, and the difference of air mass fraction ($W-W_\infty$) through the boundary layer varying from near 0.0 to 0.45 (corresponding to the temperature difference varying from 0.0 to 50.0 °C). Gebhart's [22] estimate of a ratio of contribution equal to 1/3 from 10.0 °C temperature difference is in agreement with these results. The temperature contribution to the buoyancy force can be more than 50% of the concentration contribution for larger temperature differences and should be taken into account.

To account for the contribution from thermal expansion, the buoyancy force can be represented by combining Eqs. (26) and (27) as

$$\frac{\rho-\rho_\infty}{\rho}=\left(1+\frac{M_{m\infty}}{M_g-M_v}\frac{P_t v_{fg}}{h_{fg}}\right)\beta^*(W-W_\infty)=\beta^+(W-W_\infty) \tag{28}$$

which can be substituted into the momentum equation without violating the similarity assumption.

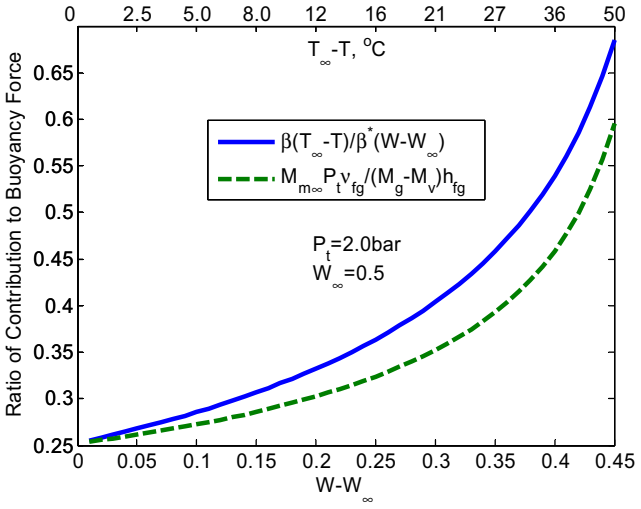

Fig. 2. Temperature and concentration contributions to buoyancy force.

3. Results

3.1. Heat transfer enhancement due to bulk velocity

Figs. 3 and 4 show the typical velocity and gas mass fraction profiles, respectively, along the dimensionless distance from the two-phase interface (η), ($Sc = 0.5$, $W_\infty = 0.05$, c_{pL} $(T_i - T_w)/(h_{fg}\mathrm{Pr}_L) = 0.002$, and $[\rho_L\mu_L/(\rho\mu)]^{1/2} = 150$). The gas component is represented by air in producing Figs. 3 and 4. The profiles are influenced by a varying amount of superimposed forced convection on the basic natural convection process, indicated by the Re^2/Gr^* parameter, and hence the ξ parameter according to Eq. (6). The profile of the dimensionless velocity was obtained from the solution of f' and Eq. (9):

$$\frac{u}{(4gx\beta^*)^{1/2}} = \frac{f'}{\xi^2} \tag{29}$$

and the profile for the air mass fraction came from the solution of ϕ.

As the bulk velocity indicated by the Re^2/Gr^* parameter increases, the velocities at the boundary layer also increase (Fig. 3) and superimposed forced convection tends to sweep away some gas previously accumulated at the interface (Fig. 4) and to increase the interfacial temperature so that condensation driving force is also increased. Hence, the mechanism for superimposed forced convection to enhance condensation heat transfer of the basic natural convection process was found analytically. This mechanism suggests that the mixed convection effects not only depend on the relative magnitude of forced to natural convection, but also on the bulk flow capability to blow away non-condensable gas accumulated at the interface. The criterion for transition from natural to mixed convection will be developed in a later subsection based on this finding.

Recently, Debbissi [7] studied the effects of the bulk velocity on water evaporation into humid air and found that the bulk velocity reduced the mass boundary layer thickness, which results in increased evaporation due to the bulk velocity. For the condensation mass boundary layer, the thickness is also reduced when the bulk velocity enhances condensation mass transfer as shown in Fig. 5. While in Debbissi's work the mass concentration profiles were presented in two-dimensional form, the profiles in the current work are presented in one-dimensional form due to the similarity solution. For both the evaporation and condensation processes, the superimposed bulk velocity increases the gradient of the mass concentration at the two-phase interface, resulting in enhancement of mass transfer.

3.2. Comparison with experiments and theory

Experiments with condensation from steam–air mixtures along a vertical plate were performed by Anderson [23]. In the experiments the rectangular test vessel was scaled down by a factor of 12 from the prototypical containment, with a vertical aluminum condensing plate installed at the top of one vertical wall in the test vessel and insulated polycarbonate plates installed on each of other three vertical walls where little condensation took place. The steam was supplied by a system producing a uniform distribution of steam inflow across the bottom of the test vessel at low velocities. The flow pattern induced by condensation on only one of the four vertical walls and the resulting buoyancy force [23] was similar to the one schematically depicted in Fig. 1. The test facility was first flushed with air and then steam was allowed to enter the test section with a steam flow rate adjusted to obtain the desired temperature and pressure in the test section. The temperature and flow rate of the coolant on the other side of the condensing plate were also adjusted as the test section approached a steady state. During the steady state two independent methods

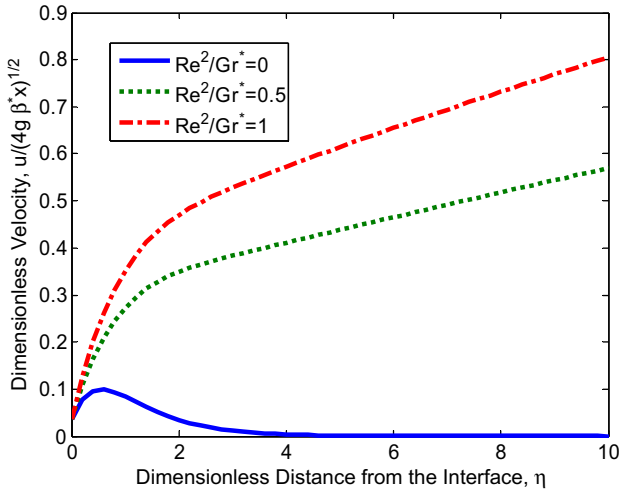

Fig. 3. Velocity profiles.

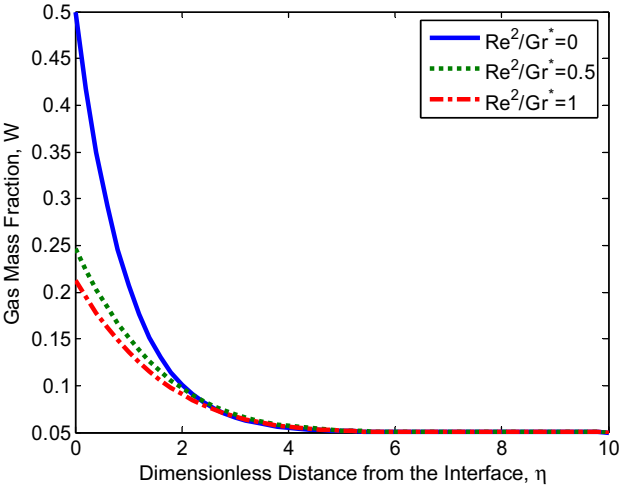

Fig. 4. Gas mass fraction profiles.

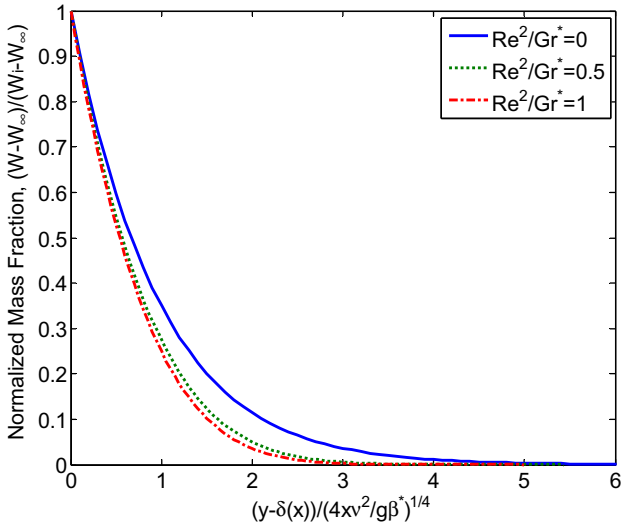

Fig. 5. Dimensionless gas mass fraction profile.

for the heat transfer coefficient measurement were used, one using thermocouples to measure the local heat flux, the other using the coolant energy balance to determine the area-averaged heat transfer coefficient. The agreement between these two methods was within the error band of the individual measurement [23], therefore no attempt is tried to differentiate the data resulting from two independent measurement methods when comparing to the theoretical predictions.

Condensation heat transfer coefficients from the gas bulk to the wall, averaged for the entire vertical plate with a length of 0.91 m, were measured in the experiments. These experimental heat transfer coefficients are used to validate the analytic values predicted with Eq. (15). Two test series performed at atmospheric pressure were compared to the current analysis. The steam–gas bulk temperature ranged from about 335 to 363 K, and the temperature difference between the gas bulk and wall ranged from about 10 to 60 K. It is estimated that the Grashof number in these two tests is of moderate magnitude, on the order of 10^9, or in the laminar to transition range where turbulent effects are insignificant. The first test series were performed under constant wall temperatures, while the gas bulk temperatures were varied to obtain both a varying bulk gas concentration and a varying temperature difference between the wall and gas bulk. The second test series were performed under constant gas bulk temperatures and varying wall temperatures.

In Figs. 6 and 7, analytic results assuming $Sc = 0.55$ for vapor–air mixtures were compared to the first and second test series, respectively, wherein (a) the solid lines represent analytic results calculated from the current mixed convection condensation model ($0 < \xi < 1$) with the buoyancy force approximated by Eq. (28) accounting for both concentration and temperature contributions; (b) the dashed lines represent those calculated from the current natural convection model ($\xi = 1$) with the buoyancy force also approximated by Eq. (28); (c) the dotted lines represent those calculated using Sparrow's theory [1] for natural convection with the buoyancy force approximated by Eq. (4) only accounting for the concentration contribution; and (d) the error bars indicate 15% of experimental error.

Several important points are raised in Figs. 6 and 7. First, both experiments and theoretical analysis show that heat transfer coefficient increases with the temperature difference between the gas bulk and wall for the first test series, while the inverse is true for the second test series. In the first test series (Fig. 6) with a constant

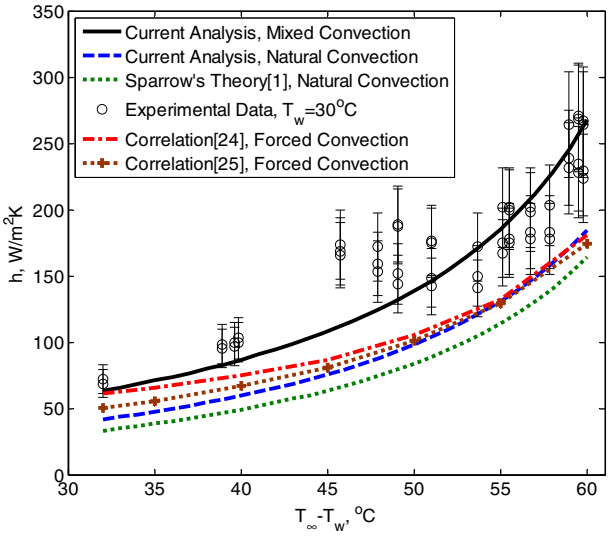

Fig. 6. Comparison with experiments [23] under constant wall temperatures.

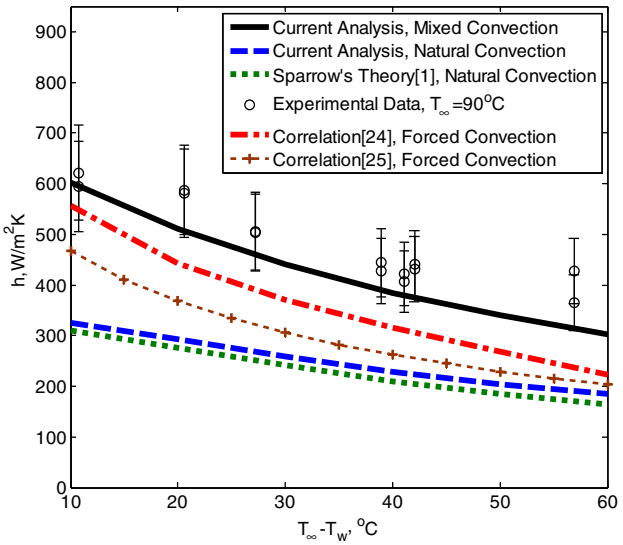

Fig. 7. Comparison with experiments [23] under constant bulk temperatures.

wall temperature, a decrease of the bulk gas concentration due to an increase of the bulk temperature results in increase of both the heat flux and temperature difference, however, the heat flux increases with a higher rate than the temperature difference. Therefore, the heat transfer coefficient increases with increasing temperature difference. Even though the heat flux increases with the temperature difference in the second test series (Fig. 7), the temperature difference increases at a higher rate. Therefore, heat transfer coefficients decrease with increasing temperature difference.

Second, accounting for both temperature and concentration contributions to the buoyancy force in the current work leads to a higher prediction (in dashed curves) of condensation heat transfer coefficients than that (in dotted curves) predicted by Sparrow's theory [1], in which contribution from thermal expansion to the buoyancy force was neglected. However, analytic results based on natural convection from both the current analysis and Sparrow's theory [1] underpredicted all experimental data, which implies effects of superimposed forced convection caused by the bulk velocity were significant in the experiments.

Third, effects of superimposed forced convection in the first test series were less significant than those in the second test series. This point can be verified by comparing experimental condensation heat transfer coefficients in two test series for test conditions with roughly the same wall temperature (30 °C) and bulk temperature (90 °C) in Figs. 6 and 7: superimposed forced convection induced a lower heat transfer coefficient in the first test series (about 250 W/m^2 K) than that in the second series (about 350 W/m^2 K) even though they had almost the same bulk air mass fraction and buoyancy force. Since the bulk velocity was not measured in the experiments, the magnitude of superimposed forced convection was unknown. Therefore, a strict comparison with experiments is not possible. Nonetheless, parametric studies were carried out to demonstrate the significance of mixed convection in the experiments. The current analysis assumed $Re/\sqrt{Gr^*} = 1.4$ ($\xi = 0.4568$) in the mixed convection model to compare with data in the first test series, while $Re/\sqrt{Gr^*} = 2.0$ ($\xi = 0.4142$) was assumed to compare with data in the second test series which has more significant mixed convection effects as stated before. The solid lines in Figs. 6 and 7 represent these assumptions about the magnitude of superimposed forced convection, which demonstrate that the current model predicts the mixed convection effects consistent with experiments.

For Anderson's experimental conditions [23], a comparison of theoretical predictions for the various convective components is also shown in Figs. 6 and 7. Sparrow's model [1] evaluates the natural convection component, Groff et al. [24] and Stephan [25] predict the forced convection component and the new model presented here provides the mixed convection contribution.

Numerical solutions of the boundary layer equations in other theoretical studies are usually not in the form which can directly be used for comparison. Fortunately, Groff [24] and Stephan [25] have developed analytical solutions that correlate the numerical results of Srzic [9] and Sparrow [16], respectively. Groff [24] used an algebraic correlation for the local Nusselt number fitted from numerical results in Srzic [9]. The local Nusselt number in the algebraic correlation depends on the local Reynolds number, the gas bulk temperature and air concentration, as well as the temperature difference between the gas bulk and wall. These dependent variables are presented or implied in Figs. 6 and 7, including the local Reynolds number ($Re/\sqrt{Gr^*} = 1.4$ in Fig. 6 and $Re/\sqrt{Gr^*} = 2.0$ in Fig. 7). Therefore, the heat transfer coefficient averaged over the whole plate can be easily calculated with Groff's algebraic correlation. On the other hand, Stephan [25] developed empirical correlations based on numerical solutions of the conservation equations in Sparrow's [16] work. The correlations can be applied to determine the interfacial temperature between the liquid- and vapor-phase and hence the condensation heat transfer coefficient using an iterative algorithm. The inputs for the algorithm are the local Reynolds number, the wall temperature, and the gas bulk temperature and air concentration.

The dash-dotted and plus-dotted curves in Figs. 6 and 7 represent the theoretical predictions from Groff's [24] and Stephan's [25] correlations, respectively. Assuming identical boundary conditions, while Stephan's correlation predicts lower heat transfer coefficients than Groff's, both correlations predict lower heat transfer coefficients than the current mixed convection model, because both correlations only account for the forced convection component.

Overall, the mixed convection model developed in the current work predicts well various test data in Anderson's [23] experiments. Other theoretical models accounting for only one convective component underpredict experimental data. The comparison among the mixed convection, natural convection and forced convection modeling, as well as the experimental data justifies the mixed convection modeling approach under conditions specific to Anderson's [23] test facility and also to prototypical pressurized water reactor containment.

3.3. Transition to mixed convection regime

One important issue concerning mixed convection studies is to distinguish mixed convection from either natural or forced convection. The mixed convection effects on condensation heat transfer in the current work can be indicated by the increase of the heat transfer coefficient, $(h_\xi - h_0)/h_0$, where h_ξ and h_0 denote the condensation heat transfer coefficient for mixed and natural convection flow, respectively. The flow conditions are identical for evaluation of h_ξ and h_0 except for a varying amount of superimposed velocity associated with h_ξ. Fig. 8 illustrates the mixed convection effects against the relative magnitude of forced convection to natural convection, $Re^2/Gr = Re^2/[\beta^+(W_i - W_\infty)Gr^*]$, for a variety of bulk air mass fractions (W_∞) and temperature differences between the gas bulk and wall ($T_\infty - T_w$). The cases for Fig. 8 assume a total pressure of 2.0 bar and $Sc = 0.55$. Further numerical results which are not shown herein for the total pressure between 1.0 and 3.0 bar, and the Schmidt number between 0.5 and 0.6, demonstrate that, while the total pressure or the Schmidt number in these ranges may influence h_ξ or h_0 appreciably, their influence on the ratio of h_ξ to h_0 is negligible. Therefore, the cases in Fig. 8 represent a wide range of flow conditions.

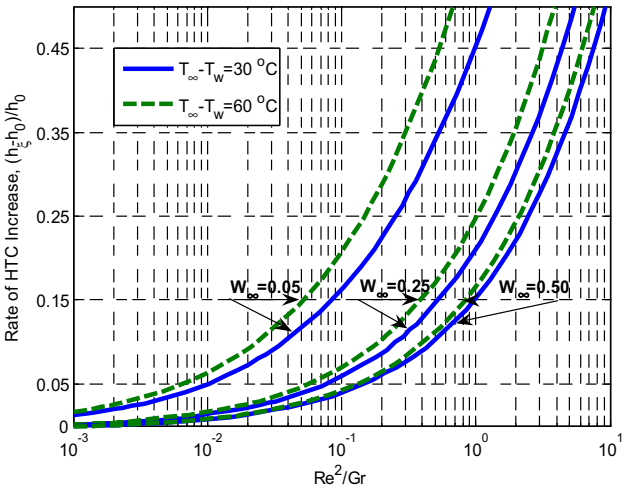

Fig. 8. Mixed convection effects on heat transfer coefficients.

Fig. 8 illustrates that, unlike single-phase flow where the mixed convection effects on heat transfer only vary with the relative magnitude of forced convection to natural convection, the mixed convection effects for condensation from steam–gas flow also vary with bulk gas mass fractions and temperature differences between the bulk and wall. Sparrow [3] suggested that a 5% increase of heat transfer coefficient could be used to indicate the presence of non-negligible mixed convection effects. Also from Fig. 8, corresponding to a 5% increase of the heat transfer coefficient, Re^2/Gr is not a unique value any more as in the analysis of single-phase heat transfer [3]. The value of Re^2/Gr spans a wide range of almost two orders of magnitude and can be as low as 0.006 and as high as 0.2, depending on bulk gas mass fractions and temperature differences. Therefore, characterization of the mixed convection effects by reading Fig. 8 still depends on several input variables. The next paragraphs discuss a way to simplify the characterization of the mixed convection effects based on the physical mechanism found in the current work.

Fig. 8 demonstrates that superimposed forced convection induces higher increases of the heat transfer coefficient for greater temperature differences and lower bulk gas mass fractions, while other parameters are unchanged. This observation can be explained by the previously discussed mechanism of heat transfer enhancement by superimposed forced convection in Section 3.1 (the bulk flow blows away some non-condensable gas previously accumulated near the interface to enhance condensation heat transfer), and a concept introduced herein about the bulk flow blowing capability. As inferred from Fig. 8, when the gas mass fraction difference between the interface and bulk (or temperature difference) is large and the bulk gas mass fraction is low, the bulk flow with a fixed relative magnitude of forced to natural convection (Re^2/Gr) tends to be more capable of blowing gas away from the interface and results in higher heat transfer enhancement. Therefore, it is postulated that the bulk flow blowing capability can be characterized by:

$$B_m = \frac{W_i - W_\infty}{W_\infty} \tag{30}$$

which is exactly the same as the definition of the conventional mass transfer driving potential [26].

Obviously, both the bulk flow blowing capability indicated by B_m and the forced convection magnitude indicated by Re contribute to the mixed convection effects over the basic natural convection

process indicated by Gr. Therefore, the results in Fig. 8 are recast in Fig. 9, where the rate of increase of heat transfer coefficient is plotted against a new parameter: $B_m Re^2/Gr$.

When results in Fig. 8 are scaled by B_m along the horizontal coordinate, the curves in Fig. 8 cluster together and the six curves become difficult to differentiate. Therefore, to avoid ambiguity, the curves in Fig. 9 are divided into three groups according to the respective gas bulk mass fraction. While there is a unique horizontal axis in Fig. 9, the vertical axis is offset by 0.0, 0.1, and 0.2 for the curves with the gas bulk mass fraction of 0.05, 0.25, and 0.50, respectively.

If 5% for the increase of heat transfer coefficient can be used to indicate non-negligible mixed convection effects on the basic natural convection process [3], the criterion for transition from natural to mixed convection for steam–gas flow condensing along a vertical plate can be derived by interpreting results in Fig. 9. This is of practical importance to the heat and mass transfer analogy approach in engineering calculations, where a convection-regime dependent correlation must be decided [27]. In contrast to Fig. 8, Fig. 9 shows that corresponding to a 5% increase of the heat transfer coefficient, the value of the horizontal coordinate ($B_m Re^2/Gr$) is almost invariant with the bulk gas mass fraction and the temperature difference, and hence a quite simple criterion can be derived to indicate transition from natural to mixed convection:

$$B_m Re^2/Gr > 0.15 \tag{31}$$

4. Conclusions

A new method has been developed to analyze condensation of steam–gas mixed convection flow along a vertical plate. The local similarity method is used to reduce the dimensions of the multivariable problem. The new mixed convection model accounts for both concentration and temperature contributions to the buoyancy force, and uses a mixed convection parameter to represent varying degrees of forced convection superimposed on the natural steam–gas flow. The new method was shown to predict results consistent with experiments. The mechanism for superimposed forced convection assisting heat transfer of the basic natural convection process was demonstrated: some gas previously accumulated near the two-phase interface is blown away by the superimposed bulk velocity, resulting in an elevated condensation driving force. This mechanism suggests that the bulk flow blowing capability plays a role in quantification of the mixed convection effects. Consequently, the bulk flow blowing capability, which can be characterized by the mass transfer driving potential (B_m), and the relative magnitude of forced to natural convection (Re^2/Gr) are used to facilitate identification of convection regimes. A simple criterion was developed to indicate transition to mixed convection regime from a natural convection steam–gas flow condensing along a vertical plate: $B_m Re^2/Gr > 0.15$. The criterion found in the current work has practical applications in the heat and mass transfer analogy approach for engineering calculations, where a convection-regime dependent correlation must be decided.

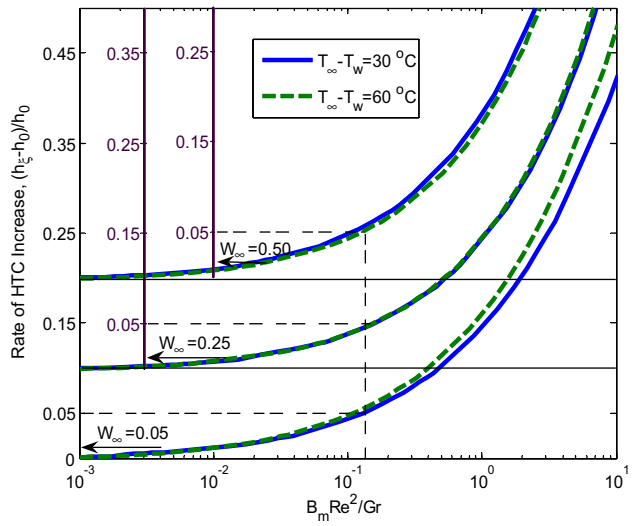

Fig. 9. Recasting of Fig. 8 using B_m to scale the horizontal axis.

Appendix A. Contribution of thermal expansion to buoyancy force

Upon using the Clausius–Clapeyron equation, $(T_\infty - T)/(P_{v\infty} - P_v) = \overline{T} v_{fg}/h_{fg}$, and the definition of the steam volumetric fraction, $x_v = P_v/P_t$, Eq. (26) can be rewritten as

$$\frac{\rho - \rho_\infty}{\rho} = \beta^*(W - W_\infty) + \frac{\beta \overline{T} P_t v_{fg}}{h_{fg}}(x_{v\infty} - x_v) \tag{A1}$$

Upon using the relation between the steam volumetric fraction and the gas mass fraction (W), $x_v = (1 - W)M_m/M_v$, the definition of the mixture molecular weight, $M_m = M_g M_v/[(1 - W)M_g + WM_v]$, the definition of β^* in Eq. (5), and $\beta\overline{T} \approx 1$, Eq. (A1) can be converted to

$$\frac{\rho - \rho_\infty}{\rho} = \beta^*(W - W_\infty) + \frac{M_m}{M_g - M_v}\frac{P_t v_{fg}}{h_{fg}}\beta^*(W - W_\infty) \tag{A2}$$

Upon using Eq. (4) and substituting the series expansion of M_m in terms of $\beta^*(W - W_\infty)$, Eq. (A2) can be expanded to

$$\frac{\rho - \rho_\infty}{\rho} = \beta^*(W - W_\infty) + \frac{1}{M_g - M_v}\frac{P_t v_{fg}}{h_{fg}}\beta^*(W - W_\infty)M_{m\infty} [1 + \beta^*(W - W_\infty) + \cdots] \tag{A3}$$

Again, retaining the linear terms about $(W - W_\infty)$ and neglecting terms with higher orders [22], the buoyancy force with contribution from both temperature and concentration effects can be approximated as

$$\frac{\rho - \rho_\infty}{\rho} \approx \beta^*(W - W_\infty) + \frac{M_{m\infty}}{M_g - M_v}\frac{P_t v_{fg}}{h_{fg}}\beta^*(W - W_\infty) \tag{A4}$$

References

[1] E.M. Sparrow, S.H. Lin, Condensation heat transfer in the presence of noncondensable gas, ASME J. Heat Transfer 86 (1964) 430–436.
[2] W.J. Minkowycz, E.M. Sparrow, Condensation heat transfer in the presence of noncondensables, interfacial resistance, superheating, variable properties, and diffusion, Int. J. Heat Mass Transfer 9 (1966) 1125–1144.
[3] E.M. Sparrow, R. Eichhorn, J.L. Gregg, Combined forced and free convection in a boundary layer flow, Phys. Fluids 2 (1959) 319–328.
[4] T.S. Chen, E.M. Sparrow, A. Mucoglu, Mixed convection in boundary layer flow on a horizontal plate, ASME J. Heat Transfer 97 (1977) 66–71.
[5] V.E. Denny, A.F. Mills, V.J. Jusionis, Laminar film condensation from a steam–air mixture undergoing forced flow down a vertical surface, ASME J. Heat Transfer 91 (1971) 297–304.
[6] V.E. Denny, V.J. Jusionis, Effects of noncondensable gas and forced flow on laminar film condensation, Int. J. Heat Mass Transfer 15 (1972) 315–326.
[7] C. Debbissi, J. Orfi, S. Ben Nasrallah, Evaporation of water by free or mixed convection into humid air and superheated steam, Int. J. Heat Mass Transfer 46 (2003) 4703–4715.
[8] K. Lucas, Combined body force convection in laminar film condensation of mixed vapours – integral and finite difference treatment, Int. J. Heat Mass Transfer 19 (1976) 1273–1280.
[9] V. Srzic, H.M. Soliman, S.J. Ormiston, Analysis of laminar mixed-convection condensation on isothermal plates using the full boundary layer equations: mixture of a vapor and a lighter gas, Int. J. Heat Mass Transfer 42 (1999) 685–695.
[10] E.C. Siow, S.J. Ormiston, H.M. Soliman, Fully coupled solution of a two-phase model for laminar film condensation of vapor–gas mixtures in horizontal channels, Int. J. Heat Mass Transfer 45 (2002) 3689–3702.

[11] S. Oh, S.T. Revankar, Boundary layer analysis for steam condensation in a vertical tube with noncondensable gases, Int. J. Heat Exchangers 6 (2005) 1–31.
[12] J.R. Lloyd, E.M. Sparrow, Combined forced and free convection flow on vertical surfaces, Int. J. Heat Mass Transfer 13 (1970) 434–438.
[13] W.J. Minkowycz, E.M. Sparrow, Local nonsimilar solutions for natural convection on a vertical cylinder, ASME J. Heat Transfer 96 (1974) 178–183.
[14] A. Dehbi, M.W. Golay, M.S. Kazimi, Theoretical modeling of the effects of noncondensable gases on steam condensation under turbulent natural convection, AIChE Proc. Natl. Heat Transfer Conf. (1991) 29–38.
[15] C.M. Winkler, T.S. Chen, Mixed convection in film condensation from isothermal vertical surfaces – the entire regime, Int. J. Heat Mass Transfer 43 (2000) 3245–3251.
[16] E.M. Sparrow, W.J. Minkowycz, M. Saddy, Forced convection condensation in the presence of noncondensables and interfacial resistance, Int. J. Heat Mass Transfer 10 (1967) 1829–1845.
[17] E.P. Volchkov, V.V. Terekhov, V.I. Terekhov, A numerical study of boundary-layer heat and mass transfer in a forced flow with humid air with surface steam condensation, Int. J. Heat Mass Transfer 47 (2004) 1473–1481.
[18] E.M. Sparrow, W.J. Minkowycz, Buoyancy effects on horizontal boundary-layer flow and heat transfer, Int. J. Heat Mass Transfer 5 (1962) 505–511.
[19] I.G. Shekriladze, V.L. Gomelauri, Theoretical study of laminar film condensation of flowing vapor, Int. J. Heat Mass Transfer 9 (1966) 581–591.
[20] M.S. Raju, X.Q. Liu, C.K. Law, A formulation of combined forced and free convection past horizontal and vertical surfaces, Int. J. Heat Mass Transfer 27 (1984) 2215–2224.
[21] Y. Liao, Modeling condensation with a noncondensable gas for mixed convection flow, Ph.D. Thesis, Purdue University, West Lafayette, IN, 2007.
[22] B. Gebhart, L. Pera, The nature of vertical natural convection flows resulting from the combined buoyancy effects of thermal and mass diffusion, Int. J. Heat Mass Transfer 14 (1971) 2025–2050.
[23] M.H. Anderson, Steam condensation on cold walls of advanced PWR containments, Ph.D. Thesis, University of Wisconsin, Madison, WI, 1998.
[24] M.K. Groff, S.J. Ormiston, H.M. Soliman, V. Srzic, O.A. Ramirez-Iraheta, An algebraically-explicit correlation for forced-convection condensation of steam–air and steam–hydrogen on horizontal plates, Int. Commun. Heat Mass Transfer 29 (2002) 1047–1056.
[25] K. Stephan, Interface temperature and heat transfer in forced convection laminar film condensation of binary mixtures, Int. J. Heat Mass Transfer 49 (2006) 805–809.
[26] M.K. Kays, M.E. Crawford, Convective Heat and Mass Transfer, second ed., McGraw-Hill, New York, 1993. pp. 348–357.
[27] Y. Liao, Y.K. Vierow, A generalized diffusion layer model for condensation of vapor with noncondensable gases, ASME J. Heat Transfer 129 (2007) 988–994.